Physical Biology

PAPER

# Neutral dynamics and cell renewal of colonic crypts in homeostatic regime

RECEIVED
22 September 2017

REVISED
14 December 2017

ACCEPTED FOR PUBLICATION
30 January 2018

PUBLISHED
1 March 2018

A J Fendrik[1,2,3], L Romanelli[1,2] and E Rotondo[1]

[1] Instituto de Ciencias, Universidad Nacional de General Sarmiento-J.M.Gutierrez 1150, (1613) Los Polvorines, Buenos Aires, Argentina
[2] Consejo Nacional de Investigaciones Científicas y Técnicas- Buenos Aires, Argentina
[3] Author to whom any correspondence should be addressed.

**E-mail:** afendrik@ungs.edu.ar, lili@ungs.edu.ar, erotondo@ungs.edu.ar

**Keywords:** stem cells, colonic crypts, stochastic cell renewal, symmetric division, neutral drift

## Abstract

The self renewal process in colonic crypts is the object of several studies. We present here a new compartment model with the following characteristics: (a) we distinguish different classes of cells: stem cells, six generations of transit amplifying cells and the differentiated cells; (b) in order to take into account the monoclonal character of crypts in homeostatic regimes we include symmetric divisions of the stem cells. We first consider the dynamic differential equations that describe the evolution of the mean values of the populations, but the small observed value of the total number of cells involved plus the huge dispersion of experimental data found in the literature leads us to study the stochastic discrete process. This analysis allows us to study fluctuations, the neutral drift that leads to monoclonality, and the effects of the fixation of mutant clones.

## 1. Introduction

The cell renewal dynamics in Lieberkühn crypts located in the intestinal epithelium have been the object of many experimental and theoretical studies. This is due to the fact that anomalies and disruptions in their functioning are related with the development of colonic cancer, as well as the need to clarify the rhythm of cellular divisions in the homeostatic regime to ensure the tissue's renewal.

Indeed, in multicellular organisms, cell divisions from stem cells (SCs) of different lineages must provide the necessary number of cells for proper functioning, in order to get an adequate cell renewal and/or reconstruction in case of damage (or development during embryogenesis) for the different tissues.

The strategies and rhythm of mitosis must be adapted to the requirements for each specific case. For instance, during embryonic development, as a rule, the first mitosis must create a sufficient number of SCs (through SC–SC symmetric divisions) to guarantee high production of various cell types at later times when asymmetric divisions (SC–differentiated) take place in the intermediate stages [1]. The symmetric (differentiated–differentiated) divisions in the final stage are those that prevail [2, 3].

Cell renewal in the homeostatic regimen is quite different. Here, the process must lead to a stable (although fluctuating) population of cells of various types, to compensate the disappearance of differentiated cells produced in their normal stage [4].

Colonic crypts are finger-shaped formations where the renewal processes take place. At the bottom of each crypt there is a small set of SCs that gives origin to a set of cells, known as transit amplifying cells (TACs), that perform between four and six divisions [5–7] before the differentiated cells of the lineage are generated (secretory lineages: goblet cells, enteroendocrine cells; and absorptive lineage: enterocytes). As TACs proliferate, committing themselves more and more to their final fate, they migrate from the bottom of the crypt to its mouth, so that the already differentiated ones end up being lost at the intestinal lumen. In the small intestine, the SCs originate another type of secretory cell (Paneth cells) that migrates towards the bottom of the crypt. Paneth cells are absent or rare in the colon [8], and their lifetime is somewhat longer than the other phenotypes of the lineage [10]. Wnt signaling in the crypts maintains the stem cell population [9], whereas Notch signaling leads to the diversification of stem cells, progeny and controls the number that is committed to a secretory or absorptive fate [10, 11].

Today's techniques provide many observations in mice, so in the present work we focus on them. One striking aspect of the experimental results is the huge dispersion of data reported by various authors. For

example: [5] establish that the number of SCs per crypt is between 4 and 16; [12] reports between 4 and 8; [13] reports 4; [14] between 1 and 40 and [15, 16] between 4 and 6. The same pattern reappears concerning the total number of cells per crypt ([5]: 235–250; [17], 300).The fraction of proliferative cells by crypt is 2/3 in [5], between 1/2 and 4/5 in [13], 1/5 in [18] and 1/3 in [19] and [20]. We could follow the list regarding the duration of the cell cycle of the SC, TAC and so on.

Although this fact could be explained by the fact that the experimental techniques and the markers for the genes that identify the SCs are different, it seems to us that it implies that fluctuations in the population of the crypt in the homeostatic regimen are important. These fluctuations may be related to the stochastic character of the cell fate [4]. Cell fate is determined by various biochemical processes (inherently stochastic) that occur inside the cell, as well as by fluctuations that occur outside it (viz. interaction with other cells, external gradients, etc) [21]. Generally these sources of noise are called as intrinsic and extrinsic respectively. When there are fluctuations in the system, they are a feature of the system, and their study and measurement become as important as the determination of the mean behavior. Similarly, any theoretical approach for these systems should take into account the fluctuations. The theoretical approaches with which these phenomena are addressed are extensively reviewed in [22].

There is an interesting observation regarding the dynamics in the crypt. Strong evidence has been found indicating its monoclonal character: that is, in a homeostatic regime, all the cells of the crypt are descendants of a single SC [23–26]. By using a crypt model with mechanical interactions [27, 28], the transit to monoclonality has been studied through computer simulations [29]. In this context, it is natural to describe this dynamics as a Moran process [30]. Basically, this stochastic process consists of a random substitution produced by joint events of disappearance of a SC (through a TAC–TAC symmetric division) followed by the birth of another SC (SC–SC symmetric division) in a set of $N$ stem cells, where $N$ is fixed. Possible asymmetric SC–TAC divisions do not affect the clonal composition of the crypt—they only produce a delay in the transit to monoclonality.

However, this type of model is incompatible with the assumption that $N$ could fluctuate in homeostatic conditions, since each stochastic event (disappearance–birth) preserves $N$. For example, two or more disappearances (births) in a row are not considered.

On the other hand, it has been speculated recently that the subdivision of the intestinal epithelium into millions of small niches, with few stem cells, constitutes a natural barrier to the fixation of better adapted mutations (that could be cancerous), due to the fact that in small populations the neutral dynamics can prevail over the Darwinian adaptation [31]. Therefore, it is of interest to analyse the possible fixation of mutant clones in the framework of a neutral drift.

To study the dynamics of cell populations in the crypt (in homeostatic regime, cancerogenesis or damage), two kinds of mathematical models have been developed: spatial models and compartment models (see [32–35], and more recently [36, 37]).

We propose a new compartment model for colonic crypts, taking into acount only the temporal evolution of the cell populations. The model is a system of ordinary differential equations, of which the corresponding stationary solutions correspond to the mean values of the cell populations. However, given the small number of cells involved, fluctuations will be important—we simulate the stochastic process corresponding to the model by using the stochastic simulation algoritm (SSA) [22, 38]. In this way, we can study the stability of the stationary solutions, and thus guarantee that the fluctuations do not lead, for example, to the extinction of the crypt.

In section 2 we present the model for colonic crypts. Section 3 is devoted to the first two compartments (SC and TAC of first generation). In section 4 we show the results for those compartments, and study the neutral dynamics that leads to monoclonality assuming a normal crypt (that is, admitting equal fitness for all stem cells). We then assume the presence of a mutant stem cell, of various kinds, and explore its effect. Section 5 refers to the other compartments. Finally in section 6 we discuss the results, and draw some conclusions. In three appendixes, we present the SSA to simulate the stochastic process (appendix A), the nullclines of the differential equation (appendix B) and an example showing the relevance of studying the stability of compartment models in the presence of fluctuations or with the addition of intrinsic noise (appendix C).

## 2. The model

The proposed model has eight compartments. One corresponds to SC, the next six to each generation of TACs ($\mathrm{TAC}_i, i = 1 \ldots 6$) and the last to fully differentiated cells (DC).

The number of SCs ($S$) can be increased by means of SC–SC symmetric divisions with a rate of $M_{S,S}$ and by means of a cell reprogramming process (plasticity) of a $\mathrm{TAC}_1$, where $P$ is the rate of such process. The processes that decrease $S$ are: the symmetric divisions of SC giving two $\mathrm{TAC}_1$ at a rate $M_{T_1,T_1}$ and the apoptosis processes with a rate $A_S$. This leads to

$$\frac{\mathrm{d}S}{\mathrm{d}t} = M_{S,S}S - M_{T_1,T_1}S - A_S S + PT_1. \qquad (1)$$

The number of $\mathrm{TAC}_1$s ($T_1$) is increased by the $\mathrm{TAC}_1$–$\mathrm{TAC}_1$ symmetric divisions of SCs as discussed above and by the asymmetric divisions of SCs that produce a SC and a $\mathrm{TAC}_1$ at rate $M_{S,T_1}$. On the other hand, $T_1$ may decrease due to $\mathrm{TAC}_2$–$\mathrm{TAC}_2$ symmetric divisions of $\mathrm{TAC}_1$s at rate of $L_{T_1}$ and the apoptosis processes at rate $A_{T_1}$. All this leads to the equation

$$\frac{dT_1}{dt} = 2M_{T_1,T_1}S + M_{S,T_1}S - L_{T_1}T_1 - A_{T_1}T_1\,. \quad (2)$$

These two compartments ($S$ and $T_1$) are the fundamental ones, and can be considered the 'engine' of the crypt. Numbers of $TAC_2$s and $TAC_3$s are increased at a rate equal to twice the symmetric divisions of the previous generation, and their number decreases when they divide symmetrically into two cells of the subsequent generation. This is displayed as

$$\frac{dT_2}{dt} = 2L_{T_1}T_1 - L_{T_2}T_2\,, \quad (3)$$

$$\frac{dT_3}{dt} = 2L_{T_3}T_2 - L_{T_3}T_3. \quad (4)$$

For the fourth generation, in addition to the symmetrical divisions of $TAC_4$ ($TAC_5$-$TAC_5$) that feed the population of the fifth generation, the probability of complete differentiation must be considered through DC–DC symmetric divisions or DC–$TAC_5$ asymmetric divisions (these do not change the number of $TAC_4$s, but do change the number of $TAC_5$s). This is taken into account by the factors $\alpha_{T_5,T_5}$, $\alpha_{D,D}$ and $\alpha_{T_5,D}$, which are the fraction of each division mentioned above.

The processes involved in the balance for $TAC_5$s are similar to those of $TAC_4$s. In this case $\alpha'_{T_6,T_6}$, $\alpha'_{D,D}$ and $\alpha'_{T_6,D}$ are the fraction of each type of division. The last generation, $TAC_6$, only produces DCs. Therefore, this can be written as

$$\frac{dT_4}{dt} = 2L_{T_3}T_3 - (\alpha_{T_5,T_5} + \alpha_{D,D})L_{T_4}T_4\,, \quad (5)$$

$$\frac{dT_5}{dt} = (2\alpha_{T_5,T_5} + \alpha_{T_5,D})L_{T_4}T_4 - (\alpha'_{T_6,T_6} + \alpha'_{D,D})L_{T_5}T_5, \quad (6)$$

$$\frac{dT_6}{dt} = (2\alpha'_{T_6,T_6} + \alpha'_{T_6,D})L_{T_5}T_5 - L_{T_6}T_6\,. \quad (7)$$

Finally, the DC compartment is fed by the divisions of $TAC_4$s, $TAC_5$s and $TAC_6$s, and $A_D$ accounts for apoptosis or entry into the intestinal lumen:

$$\frac{dD}{dt} = 2L_6T_6 + (2\alpha_{D,D} + \alpha_{T_5,D})L_{T_4}T_4 + (2\alpha'_{D,D} + \alpha'_{T_6,D})L_{T_5}T_5 - A_DD\,. \quad (8)$$

A schematic diagram of the model is shown in figure 1.

Note that it is necessary to consider each generation of TACs in a different compartment. The division of each mother TAC produces cells that are different from it (their daughters are more committed to the differentiation process). If the divisions of TACs were to feed into the same compartment as those TACs, we would be introducing immortal TACs, contradicting their transient nature.

The system of equations (1)–(8) should lead, in the stationary regime, to a finite population for each kind of cell. It is worth mentioning that the coefficients representing the rates for each process cannot be constant. If such were the case, we would have a system of linear first order differential equations, whose general solution involves exponentially increasing populations over time. These could be eliminated with an appropriate choice of parameters. Even then, our model would be completely unsatisfactory, since any fluctuation of these parameters around those values (quite small indeed) would lead to the exponential growth of some of the populations. The solution would be structurally unstable, and thus not acceptable as a description of a biological system in a homeostatic regime [39]. Furthermore, the solution should also be stable against internal noise present in the system (see appendix C).

The number of cells that emerge from the stationary solutions of the equations are continuous, but we are dealing with discrete quantities; therefore, they must be interpreted as an average value of population temporal evolution. This behaviour may be far away from the real one if the populations involved are small, as in the crypts (see appendix C).

Equations (1) and (2)—which correspond to the SC and $TAC_1$ compartments—are strongly coupled, and feed the rest of the compartments. Thus, we will establish the parameters and the solutions for these two equations, and then let the solution evolve with the remaining six.

## 3. The SC and $TAC_1$ compartments

In this section, we will consider that the processes involved in the model are regulated by a population-dependent feedback process. As has already been mentioned, such feedback should guarantee the stability of the solution not only against parametric fluctuations, but also against intrinsic noise in the equations. This regulation is included through Hill functions as

$$M_{S,S}(S,T_1) = \frac{K_{S,S}{S_o}^n}{({S_o}^n + S^n)}\frac{T_1^n}{({T_{o1}}^n + {T_1}^n)}\,, \quad (9)$$

$$M_{T_1,T_1}(S,T_1) = \frac{K_{T_1,T_1}S^n}{({S_o}^n + S^n)}\frac{T_{o1}^n}{({T_{o1}}^n + {T_1}^n)}\,, \quad (10)$$

$$A_S(S) = \frac{\lambda S^n}{({S_o}^n + S^n)}\,, \quad (11)$$

$$P(S) = \frac{\beta {S_o}^n}{({S_o}^n + S^n)}\,, \quad (12)$$

$$M_{S,T_1} = K_{S,T_1}\,, \quad (13)$$

$$L_{T_1}(T_1) = \frac{\beta' {T_1}^n}{({T_{o1}}^n + {T_1}^n)}\,, \quad (14)$$

$$A_{T_1}(T_1) = \frac{\lambda' {T_1}^n}{({T_{o1}}^n + {T_1}^n)}\,. \quad (15)$$

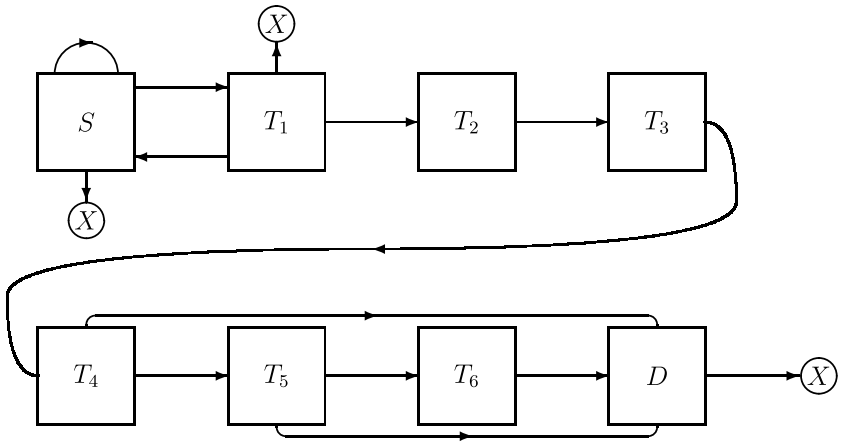


**Figure 1.** Schematic diagram of the model.

Here, $K_{S,S}, K_{T_1,T_1}, K_{S,T_1}, S_o, T_{o1}, \lambda, \lambda', \beta, n$ are parameters to be determined. Let us remark that the rate of SC-$TAC_1$ asymmetric division is taken as a constant (i.e. not regulated, or much less regulated than the other processes considered), since this process does not change the number of SCs. We have taken the same exponent $n$ for all Hill functions, and its value will be determined as the smallest integer that leads to a stable solution, resistant to the internal noise.

The other parameters will be chosen in such a way that the number of SC ($S_s$) and $TAC_1$ ($T_{s1}$) for the stationary solution are close to 15 for each case. The rate of cell division for the SC for the stationary solution results 1/24 h. That is,

$$M_{S,S}(S_s, T_{s1}) + M_{T_1,T_1}(S_s, T_{s1}) + K_{S,T_1} \approx \frac{1}{24\ \text{h}}. \quad (16)$$

The rate of cell division of $TAC_1$ is 1/19 h for the same stage, that is:

$$L_{T_1}(T_{s1}) + P(S_s) \approx \frac{1}{19\ \text{h}}\ . \quad (17)$$

The cell cycle length of $TAC_1$ is much higher than those reported in the literature (10–12 h). It is not clear that these determinations refer to $TAC_1$. We assume that it is an average of the cell cycle length of the six generations of TACs. Later, in section 5 when the parameters are defined for the other compartments, we will adjust them so that the average TAC cell cycle length equals 10 h.

A fundamental issue considered here is the speed of evolution towards monoclonality at short times. In our model, this is quite sensitive to parameter $K_{S,T_1}$ (the rate of asymmetric division). In fact, if all the divisions were of this kind, there would be no transition to the monoclonality while if were not such divisions, this transition would be very fast. This speed was measured experimentally, and for 15 initial marked SCs (15 initial clones from one SC cell each) the average number of SCs in each surviving clone is approximately six cells at 14 d [24]. $K_{S,T1}$ must be equal to zero to reproduce this result. In conclusion, in this model, the process of renovation of the crypts in the homeostatic regimen is the consequence of a regulated balance between symmetric divisions of SCs of both types (SC–SC and $TAC_1$–$TAC_1$). It is worth noting that this does not require that the divisions that lead to the disappearance of one SC ($TAC_1$–$TAC_1$) are followed by a division leading to a new SC (SC–SC). Indeed, if the stochastic process corresponding the differential equations are considered, several divisions of the same type may occur, causing large fluctuations in the populations involved.

**Table 1.** Parameters used in the calculations for equations (1) and (2).

| $K_{S,S}$ ($h^{-1}$) | $K_{T_1,T_1}$ ($h^{-1}$) | $K_{S,T_1}$ ($h^{-1}$) | $S_o$ | $T_{o1}$ | |
|---|---|---|---|---|---|
| $7.53 \times 10^{-2}$ | $9.58 \times 10^{-2}$ | 0 | 17.56 | 19 | |
| $\lambda$ ($h^{-1}$) | $\lambda'$($h^{-1}$) | $\beta$($h^{-1}$) | $\beta'$($h^{-1}$) | | $n$ |
| $1.33 \times 10^{-4}$ | $1.44 \times 10^{-4}$ | $1.1 \times 10^{-2}$ | $1.15 \times 10^{-1}$ | | 2 |

The parameters of the equations (1) and (2) necessary to obtain all the results shown below are given in table 1.

## 4. Results

### 4.1. Time evolution of populations in homeostatic regime

In this subsection, we show the results that emerge from the equations of the populations of SCs and $TAC_1$s. The solution for the differential equations has a stable fixed point ($S_s = 15, T_{s1} = 15.62$) (see appendix B.1) and it describes the behavior of the average population in homeostatic conditions. The stochastic simulation corresponding to the stochastic process that emerges from these differential equations is solved using an algorithm based on Gillespie's method [38] (see appendix A).

Figures 2(a) and (b) show the solution of equations (equations (1) and (2)) for the populations of SCs and $TAC_1$s as a function of time. They are displayed as thick lines parallel to the $t$ axis in each graph.

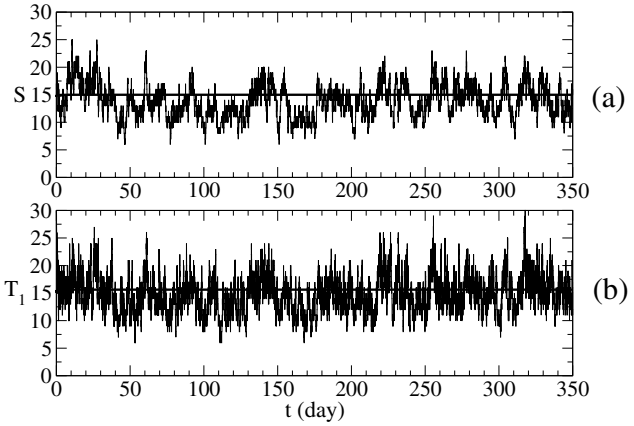


**Figure 2.** (a) Time evolution of SC population. The horizontal line in 15 corresponds to the stationary solution of the differential equations. The noisy curve around this solution corresponds to one realization obtained by considering the stochastic simulation corresponding to the stochastic process involved in the differential equations. (b) The same as in (a), but referring to the $TAC_1$ population.

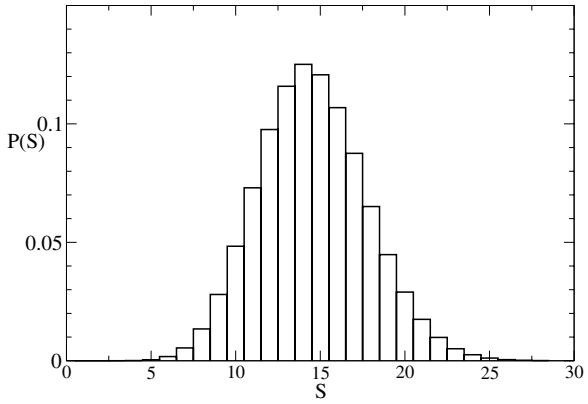


**Figure 3.** Probability distribution of SC population in homeostatic regime obtained from frequencies over $10^6$ crypts.

Also shown is a realization of the solutions obtained by using the algorithm mentioned above. It can be observed that although the populations are highly fluctuating in time, such fluctuations do not lead to the extinction of the crypt. We have tested this on $10^6$ different realizations.

To characterize these fluctuations, the probability distribution $P(S)$ for $S$ was calculated from the frequencies coming from these $10^6$ realizations. The distribution is shown in the figure 3. Its mean value, $\langle S\rangle$, and the standard deviation, $s$, are given by

$$\langle S\rangle = \sum_S SP(S) = 14.54\,, \tag{18}$$

$$s = \sqrt{\left\langle (S-\langle S\rangle)^2\right\rangle} = 3.2\,. \tag{19}$$

### 4.2. Neutral drift and transit to monoclonality

We introduce the conditional probability that cell $j$ participated in a process, given that the process has occurred. As can be observed, the total number of stem cells $S(t)$ is strongly fluctuating. Assuming that SCs are identical (equal fitness) for the processes considered in the model, the conditional probabilities for symmetric division ($TAC_1$–$TAC_1$ or SC–SC), apoptosis process etc will be

$$\begin{aligned} P_S(j/(\mathrm{SC}-\mathrm{SC})) &= \frac{1}{S(t)}\,,\\ P_S(j/(\mathrm{SC}-\mathrm{TAC}_1)) &= \frac{1}{S(t)}\,,\\ P_S(j/(\mathrm{Apop.})) &= \frac{1}{S(t)}\,; \end{aligned} \tag{20}$$

and the same for $TAC_1$:

$$\begin{aligned} P_{T_1}(j/(\mathrm{Plast.})) &= \frac{1}{T_1(t)}\,,\\ P_{T_1}(j/(\mathrm{TAC}_2-\mathrm{TAC}_2)) &= \frac{1}{T_1(t)}\,,\\ P_{T_1}(j/(\mathrm{Apop.})) &= \frac{1}{T_1(t)}\,. \end{aligned} \tag{21}$$

If at $t=0$ there are $S(t=0)=N$ with equal fitness, each of these cells gives rise to a clone. In particular, at $t=0$ there will be $T_1(t=0)=N'$ originated by SCs. We must determine how the population of their offspring evolves as time evolves. At time $t$, the total populations $S(t)$ and $T_1(t)$ can be written as

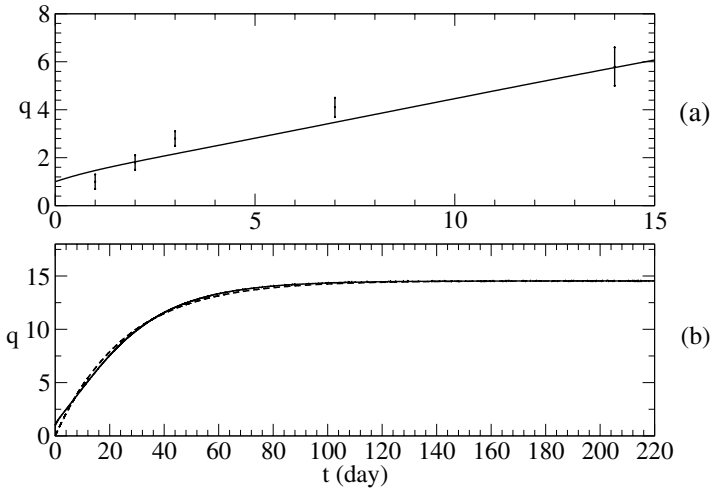


**Figure 4.** (a) Mean average size $\langle q \rangle$ as a function of time for short times. The points correspond to experimental data taken from [24]. (b) Same curve as in (a), but until times in which the homeostatic regimen has been reached (continuous curve). The dashed line curve corresponds to the best fit of the functional form $14.54(1-\exp(-t/\tau))$ ($\tau = 25.56$ d).

$$S(t) = \sum_i s_i(t), \qquad T_1(t) = \sum_i t_i(t); \tag{22}$$

where $s_i(t)$ ($t_i(t)$) are the SCs ($TAC_1$s) present at time $t$ which are descendant of each original SC. That is the $i$th clone has $s_i(t)$ SCs and $t_i(t)$ $TAC_1$s at time $t$. We can extend the above conditional probabilities for each clone involved in the process:

$$\begin{aligned} P_S(i\text{th clone}/(\text{SC}-\text{SC})) &= \frac{s_i(t)}{S(t)}, \\ P_S(i\text{th clone}/(\text{TAC}_1-\text{TAC}_1)) &= \frac{s_i(t)}{S(t)}, \\ P_S(i\text{th clone}/(\text{Apop.})) &= \frac{s_i(t)}{S(t)}, \\ P_{T_1}(i\text{th clone}/(\text{Plast.})) &= \frac{t_i(t)}{T_1(t)}, \\ P_{T_1}(i\text{th clone}/(\text{TAC}_2-\text{TAC}_2)) &= \frac{t_i(t)}{T_1(t)}, \\ P_{T_1}(i\text{th clone}/(\text{Apop.})) &= \frac{t_i(t)}{T_1(t)}. \end{aligned} \tag{23}$$

Thus, when we perform stochastic simulations, both the process that occurs at each step and the clone that participates in each case are selected at random.

We characterize the dynamics calculating two quantities as a function of time.

The average size, $q$, of clones in the SC compartment is defined by

$$q(t) = \frac{\sum_i s_i(t)}{M(t)}; \tag{24}$$

where $M(t)$ is the number of clones at times $t$. Initially, we set $q = 1$, since we have $N$ clones with one SC each. Due to fluctuations, the average size $q$ for a single crypt is also fluctuating. Therefore, we calculate its mean behavior over $10^6$ crypts $\langle q(t) \rangle$. We started with 15 SCs at $t = 0$. Figure 4 shows the time evolution of $\langle q \rangle$. Panel (a) shows $\langle q \rangle$ for short times together experimental data taken from [24]. Let us remark that the inclusion of SC-$TAC_1$ asymmetric division (i.e $K_{S,T_1} > 0$) in equation (3) decrease the slope of the curve. Panel (b) shows the complete curve.

To evaluate the characteristic time of transit to monoclonality, we have fitted the curve as

$$\langle q(t) \rangle = 14.54(1 - \exp(-t/\tau)), \tag{25}$$

where $\tau = 25.56$ d.

Another way to evaluate the transit time towards the monoclonality is by means of the calculation of the fraction of monoclonal crypts $f$ as a function of time $t$ from an ensemble of them. Figure 5 shows such fraction. To calculate the characteristic time, we have fitted the curve as

$$f(t) = \frac{t^p}{(t_m^p + t^p)}; \tag{26}$$

the best fit leads to $p = 3.04$, and the time when half of the crypts will be monoclonal is $t_m = 34.32$ d.

### 4.3. Neutral drift and mutations

The neutral drift leads to monoclonal crypts. In the results shown in the previous subsection, the initial state of the crypts had 15 distinguishable SCs and 15 $TAC_1$ (fifteen clones of one SC and one $TAC_1$ each). After evolution, the final state was monoclonal, comprising all the SCs present (and all the $TAC_1$). As the initial 15

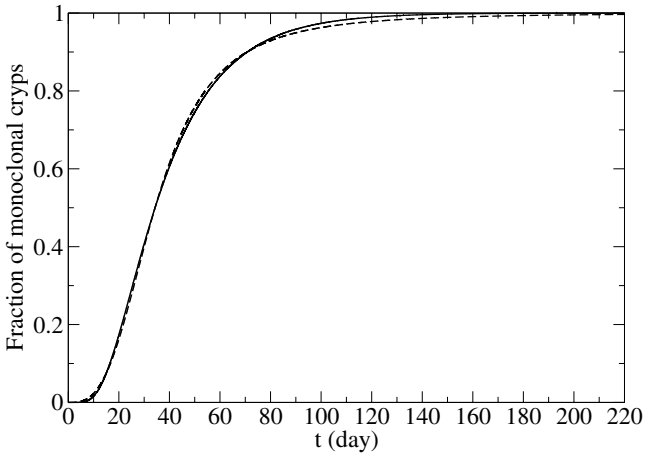


**Figure 5.** Fraction of monoclonal crypts as a function of time (continuous line curve). To determine a characteristic time, we have fitted the curve with a Hill function $(\frac{t^p}{(t_m^p+t^p)})$ with $t_m = 34.32$ d and $p = 3.04$ (dashed line curve).

clones are equally adapted, the surviving clone results from a symmetry breaking process induced by stochastic fluctuations. The relative monoclonality frequencies of each clone $f(i), i = 1, 2, \ldots, 15$ are equal, in particular $f(i) = 1/15$, as can be seen in figure 6(a).

Let us now suppose that, due to some mutation, some of the initial 15 clones have different behavior in the processes. Assuming, without loss of generality, the clone is labeled as 15. The conditional probabilities given by equation (23) are no longer valid, therefore we modify them as follows:

$$
\begin{aligned}
P_S(15\,\text{clone}/(\text{SC}-\text{SC})) &= \frac{m_1 s_{15}(t)}{\sum_{j=1}^{14} s_j(t) + m_1 s_{15}(t)}\,,\\
P_S(15\,\text{clone}/(\text{TAC}_1-\text{TAC}_1)) &= \frac{m_2 s_{15}(t)}{\sum_{j=1}^{14} s_j(t) + m_2 s_{15}(t)}\,,\\
P_S(15\,\text{clone}/(\text{Apop.})) &= \frac{m_3 s_{15}(t)}{\sum_{j=1}^{14} s_j(t) + m_3 s_{15}(t)}\,,\\
P_{T_1}(15\,\text{clone}/(\text{Plast.})) &= \frac{m_1' t_{15}(t)}{\sum_{j=1}^{14} t_j(t) + m_1' t_{15}(t)}\,,\\
P_{T_1}(15\,\text{clone}/(\text{TAC}_2-\text{TAC}_2)) &= \frac{m_2' t_{15}(t)}{\sum_{j=1}^{14} t_j(t) + m_2' t_{15}(t)}\,,\\
P_{T_1}(15\,\text{clone}/(\text{Apop.})) &= \frac{m_3' t_{15}(t)}{\sum_{j=1}^{14} t_j(t) + m_3' t_{15}(t)}\,;
\end{aligned}
\tag{27}
$$

where $m_i, m_i', i = 1, 2, 3$ are parameters related to the mutation. For the other clones $(i = 1, \ldots, 14)$ the modifications are:

$$
\begin{aligned}
P_S(i\text{th clone}/(\text{SC}-\text{SC})) &= \frac{s_i(t)}{\sum_{j=1}^{14} s_j(t) + m_1 s_{15}(t)}\,,\\
P_S(i\text{th clone}/(\text{TAC}_1-\text{TAC}_1)) &= \frac{s_i(t)}{\sum_{j=1}^{14} s_j(t) + m_2 s_{15}(t)}\,,\\
P_S(i\text{th clone}/(\text{Apop.})) &= \frac{s_i(t)}{\sum_{j=1}^{14} s_j(t) + m_3 s_{15}(t)}\,,\\
P_{T_1}(i\text{th clone}/(\text{Plast.})) &= \frac{t_i(t)}{\sum_{j=1}^{14} t_j(t) + m_1' t_{15}(t)}\,,\\
P_{T_1}(i\text{th clone}/(\text{TAC}_2-\text{TAC}_2)) &= \frac{t_i(t)}{\sum_{j=1}^{14} t_j(t) + m_2' t_{15}(t)}\,,\\
P_{T_1}(i\text{th clone}/(\text{Apop.})) &= \frac{t_i(t)}{\sum_{j=1}^{14} t_j(t) + m_3' t_{15}(t)}\,.
\end{aligned}
\tag{28}
$$

Let us remark that if we set all $m_i$ and $m_i'$ equal to one in equations (27) and (28), equations (23) are recovered.

Starting from $s_i = 1, t_i = 1, (i = 1, 2, \ldots, 15)$ and as a result of the neutral drift for large time $t$, which guarantees the establishment of homeostatic regime, we obtain $s_i(t) = 0, t_i(t) = 0, \forall i \neq k$ and $S(t) = s_k(t), T_1(t) = t_k(t)$. If $k \neq 15$, the crypt will be normal, otherwise, the crypt becomes mutant. In this case, the differential equations describing their evolution will be the same but with new parameters given by

$$
K_{S,S}^{(m)} = m_1 K_{S,S}, K_{T_1,T_1}^{(m)} = m_2 K_{T_1,T_1}, \lambda^{(m)} = m_3 \lambda,
\tag{29}
$$

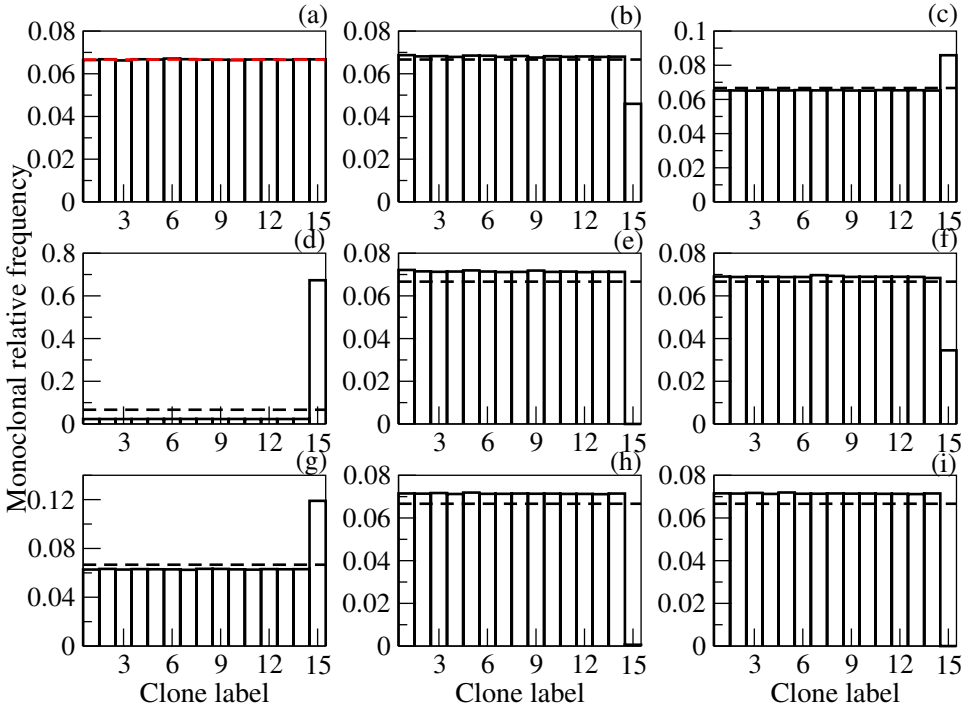


**Figure 6.** Relative fixation frequency of each clone. (a) All clones are identical. (b) Clone 15 is a mutant with $m_i = m'_i = 4, i = 1, 2, 3$. (c) Clone 15 is a mutant with $m_i = m'_i = 0.25, i = 1, 2, 3$. (d) Clone 15 is a mutant with $m_1 = 1.1, m_2 = 0.9, m_3 = m'_i, i = 1, 2, 3$. (e) Clone 15 is a mutant $m_i = m'_3 = 1, i = 1, 2, 3, m'_1 = 1.1, m'(2) = 0.9$. (f) Clone 15 is a mutant with $m_i = m'_3 = 1, i = 1, 2, 3, m'_1 = 0.9, m'_2 = 1.1$. (g) Clone 15 is a mutant with $m_i = m'_3 = 1, i = 1, 2, 3, m'_1 = 1.1, m'_2 = 0.9$. (h) Clone 15 is a mutant with $m_i = m'_2 = 1m'_3 = 1, i = 1, 2, 3, m'_1 = 0$ (see figure 7(b)). (i) The same as in (h) but for surviving crypts (see figure 7(c).

$$\beta^{(m)} = m'_1\beta, \beta'^{(m)} = m'_1\beta', \lambda'^{(m)} = m'_3\lambda'. \qquad (30)$$

This means that the fixation of a mutant clone could produce the modification of the equilibrium populations, the possible disappearance of the equilibrium or the extinction of the crypt.

In the following, we will consider seven possible mutations.

(i) $\boldsymbol{m_i = m'_i = 4, i = 1, 2, 3}$
This means that the SCs and $TAC_1$s of clone 15 are four times as 'efficient' as the other clones in all processes considered. Clearly, this mutation conspires against the fixation of the mutant clone, as can be seen in figure 6(b). The fixation of mutant clone does not change the equilibrium configuration, but the crypt renewal is faster.

(ii) $\boldsymbol{m_i = m'_i = 0.25, i = 1, 2, 3}$
In this case, the mutant clone has a quarter of the 'efficiency' of the others for all processes. This mutation favors fixation of the clone (figure 6(c)). As above, this one does not change the equilibrium configuration, but the crypt renewal is slower.

(iii) $\boldsymbol{m_1 = 1.5, m_2 = 0.5, m_3 = m'_i = 1, i = 1, 2, 3}$
Mutation increases the fraction of SC–SC mitosis and decreases the fraction of $TAC_1$–$TAC_1$ mitosis compared to the other clones. The monoclonal frequency of the mutant clone increases significantly (figure 6(d); note the scale change on the abscissa). When the monoclonal regimen is established for the mutant, the fixed point of the differential equations results ($S_s = 26.98, T_{s1} = 17.87$). Cell populations then fluctuate around these values.

(iv) $\boldsymbol{m_1 = 0.5, m_2 = 1.5, m_3 = m'_i = 1, i = 1, 2, 3}$
Mutation decreases the fraction of SC–SC mitosis and increases the fraction of $TAC_1$–$TAC_1$ mitosis compared to the other clones. The monoclonal frequency of the mutant clone decreases considerably ($2.2 \times 10^{-5}$). It is three orders of magnitude smaller than that of normal clones ($7.2 \times 10^{-2}$) (figure 6(e)). When the monoclonal regimen is established for the mutant, the fixed point of the differential equations results ($S_s = 8.4, T_{s1} = 11.22$). Cell populations then fluctuate around these values.

(v) $\boldsymbol{m_i = m'_3 = 1, i = 1, 2, 3, m'_1 = 0.9, m'_2 = 1.1}$ In this case, mutation changes the rates of $TAC_1$ rather than those of SC. The mutated $TAC_1$s of clone 15 have less plasticity and more $TAC_2$–$TAC_2$ mitosis than the others. The monoclonal frequency of the mutant clone decreases (figure 6(f)), and the fixed point is $S_s = 13.5, T_{s1} = 14$.

(vi) $\boldsymbol{m_i = m'_3 = 1, i = 1, 2, 3, m'_1 = 1.1, m'_2 = 0.9}$
As in the previous mutation, the rates of $TAC_1$s are modified, but not those of SCs. The mutated $TAC_1$s have more plasticity and less $TAC_2$–$TAC_2$

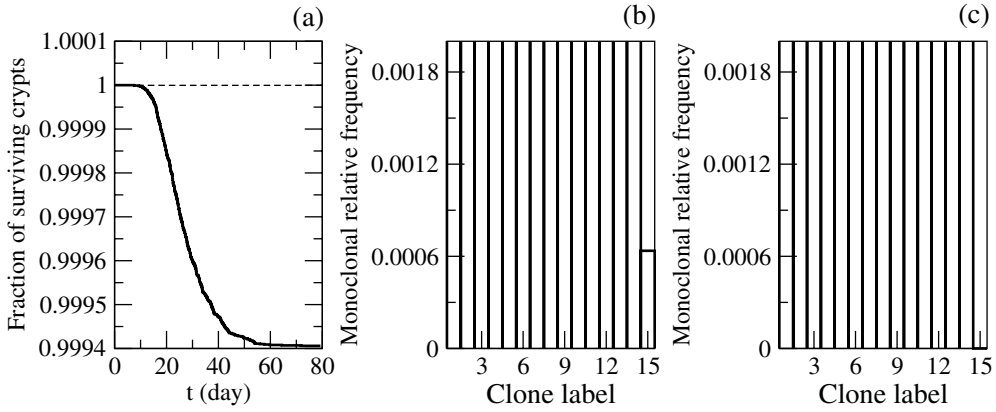


**Figure 7.** (a) Fraction of surviving crypts as a function of time when the mutant clone has no plasticity ($m_1' = 0$). The crypts that are extinguished correspond to the cases in which the mutant clone has itself imposed. (b) Graph equal to that of figure 6(h) but with a more refined scale for the abscissa. (c) Graph equal to that of figure 6(i) but with a more refined scale for the abscissa.

**Table 2.** Parameters for equations (3)–(8) and (31).

| $i$ | 2 | 3 | 4 | 5 | 6 |
|---|---|---|---|---|---|
| $\gamma_i$ ($h^{-1}$) | $3.8\times10^{-2}$ | $7.6\times10^{-2}$ | $1.69\times10^{-1}$ | $5.063\times10^{-2}$ | $1.69\times10^{-2}$ |
| $B_i$ ($h^{-1}$) | $3.8\times10^{-2}$ | $7.6\times10^{-2}$ | $1.69\times10^{-1}$ | $5.063\times10^{-2}$ | $1.69\times10^{-2}$ |
| $T_{oi}$ | 20 | 20 | 20 | 20 | 20 |

| $\alpha_{T_5,T_5}$ | $\alpha_{D,D}$ | $\alpha_{T_5,D}$ | $\alpha'_{T_6,T_6}$ | $\alpha'_{D,D}$ | $\alpha'_{T_5,D}$ | $A_D$ ($h^{-1}$) |
|---|---|---|---|---|---|---|
| 0.1 | 0.8 | 0.1 | 0.1 | 0.8 | 0.1 | 0.1 |

mitosis than the others. The monoclonal frequency increases (figure 6(g)), and the fixed point is $S_s = 16.67, T_{s1} = 17.42$

(vii) $\boldsymbol{m_i = m_2' = m_3' = 1, i = 1, 2, 3, m_1' = 0}$
In this case, the mutant loses its plasticity completely. As can be seen in figure 6(h), this produces a drastic drop in the probability of fixation of the mutant clone ($6.36\times10^{-4}$, two orders of magnitude smaller than that of normal clones: $7.14\times10^{-2}$, see figure 6(h)). In addition, unlike the previous mutations, once the mutant monoclonality is established, the crypt becomes unstable; it is extinguished shortly thereafter (see figure 6(i), which corresponds to the frequencies of surviving clones). To clarify this point in figures 7(b) and (c) we reproduce the same graphs enlarging the scale of the abscissa. Figure 7(a) shows the surviving crypt as a function of time. We can see that $6\times10^{-4}$ of the crypts are extinguished. This is the frequency of fixation for the mutant clone (as it is shown in figure 7(b)). This behavior is discussed in appendix B.2 from another point of view.

## 5. The other compartments of the crypt

In this section, we will show the results corresponding to the remaining compartments of the crypt (equations (4)–(8)), which are fed by the first two compartments.

One of the characteristics of TACs, unlike SCs, is that their offspring may not be identical to them, since each division produces cells increasingly committed to the process of differentiation. Moreover, starting from the second generation of TACs, there is no process of cell reprogramming (plasticity) able to reverse their fate.

That is why the processes that describe the equations can be compared to a slide in which $TAC_1$s enter and DCs leave. At the same time, complex processes occur through which, as a result of interactions between cells, external gradients, asymmetric inheritances and so on, it decides the final fate of each cell, giving the different phenotypes of DC that constitute the lineage.

As described in section 2, the only processes that involve changes in the $TAC_i$ populations ($i = 2, 3, \ldots, 6$) are their production from the mitosis of a TAC of previous generation and their disappearance, since their own mitosis leads to TACs of later generation or DCs. We will consider the ratios of these processes to be regulated as follows:

$$L_{T_i}(T_i) = \left(\gamma_i + \frac{B_i T_i}{(T_{oi} + T_i)}\right), i = 2, \ldots 6. \quad (31)$$

Unfortunately, we do not have experimental determinations on the equilibrium populations for each of the generations of TACs, nor about the fractions of cell divisions that originate differentiated cells in generations 4

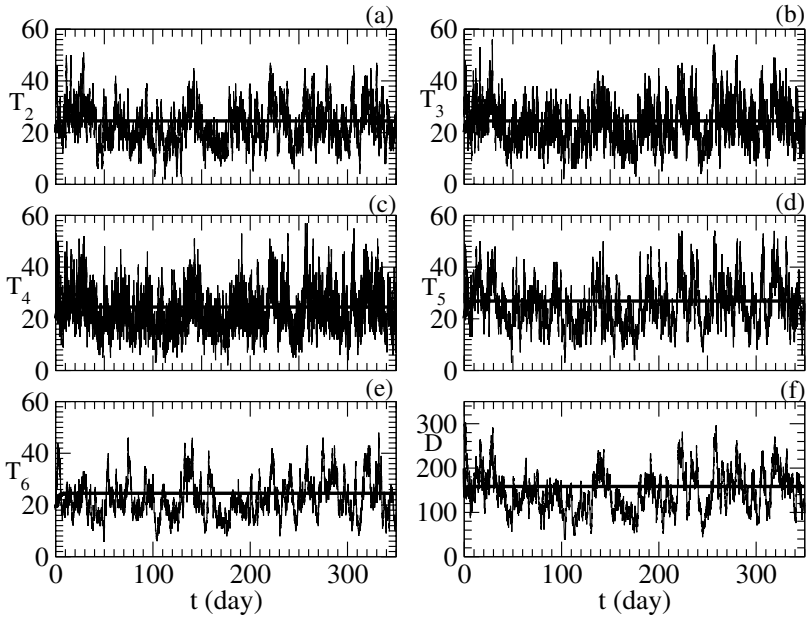


**Figure 8.** Cell populations as a function of time for: (a) $TAC_2$. (b) $TAC_3$, (c) $TAC_4$, (d) $TAC_5$ (e) $TAC_6$ (f) fully differentiated cells. The horizontal lines correspond to the equilibrium populations according with the differential equations. The fluctuating lines correspond to a realization of the stochastic simulation corresponding to the stochastic process.

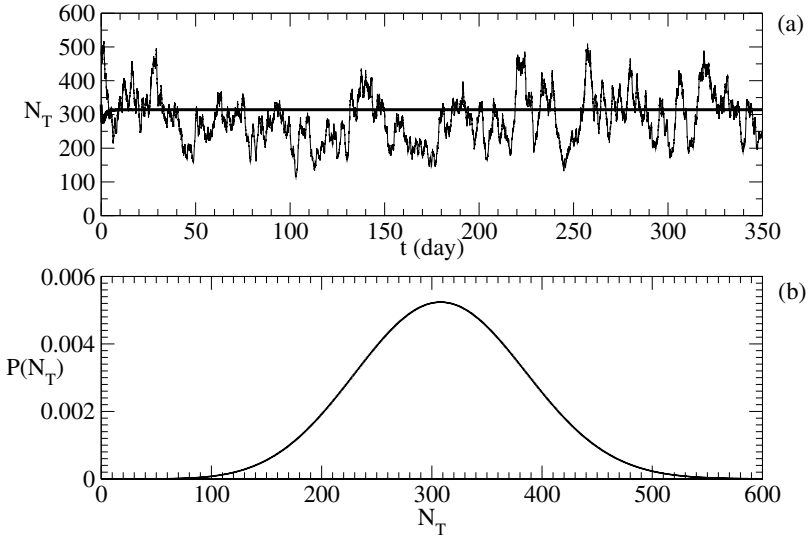


**Figure 9.** (a) Total cells in the crypt ($N_T$) versus time ($t$). The horizontal line correspond to the solution of the differential equations. The fluctuating line correspond to a realization of the SSA. (b) Relative frequency of values of $N_T$ over $10^6$ realizations.

and 5. This means that the parameters we use are not well determined and we have chosen them to satisfy the few known data. The inclusion of these results is intended to show that for a reasonable choice of parameters, there is a stable fixed point for the equations that accounts for the average cell populations, and that, moreover, these populations are stable against internal noise.

Table 2 shows the parameters used for calculations under the following criteria:

(i) The average total cell population, in homeostatic conditions comes out to 300 cells. This is:

$$S_s + \sum_{i=1}^{i=6} T_{si} + D_s = N_{sT} \approx 300\,. \tag{32}$$

(ii) The average population of DCs ($D_s$) is about 150.

(iii) The average cell cycle of all TACs is about 10 h, that is:

$$\frac{1}{\sum_{i=1}^{i=6} T_{si}} \left( (A_{T_1}(T_{s1}) + P(S_s))T_{s1} + \sum_{i=2}^{i=6} L_{T_i}(T_{si})T_{si} \right) \approx \frac{1}{10\ \text{h}}. \tag{33}$$

In such conditions the mean cell population in homeostatic conditions results $S_s = 15, T_{s1} = 15.62$ (as was already established) and $T_{s2} = 24.54, T_{s3} = 24.54, T_{s4} = 24.54, T_{s5} = 26.88, T_{s6} = 24.54, D_s = 158.41$ (stable fixed point of equations (3)–(8)). Figure 8 shows these values as well as the population for a realization of the stochastic simulation corresponding to the stochastic process. On the other hand, figure 9(a) shows the mean population of total cells ($N_{sT} = 314.06$) and the total cell population for a realization given by the stochastic simulation. Figure 9(b) shows the distribution of the total cells around the mean population.

## 6. Discussion and conclusions

In the present work, we have developed a compartment model for the evolution of the various cell populations in colonic crypts. The model consists of eight differential equations, associated with the population of SCs, TACs (six generations) and completely DCs. The equations for SC and TAC1 are coupled, and their solutions feed the other equations. The need to consider a compartment for each generation of TACs is related to the fact that these cell states are intermediate and transient. Therefore, its division necessarily leads to daughter cells qualitatively different from their progenitors (more committed to the process of cell differentiation than their progenitors).

The huge dispersion in the experimental data on the cell populations of the crypts, as well as their monoclonal character in homeostatic conditions, suggests the need to consider the equations not as differential equations but as stochastic processes that can be solved using Monte Carlo simulations. Experimental data on evolution times towards monoclonality, suggest that the cell renewal regimen in homeostasis is the result of a balance between symmetric divisions of SCs of stochastic character that introduces large fluctuations of the cell populations around their mean values. The model presented here allows study of the possible effects of mutations that can occur in some of the cells that feed the cell renewal process. The neutral drift leading to monoclonality can fix the mutant clone or extinguish it. The fixation of the mutant clones leads to atypical crypts, with different mean populations, as indication of dysfunctionalities or even the total extinction of the crypt. An example of the latter is when a mutant clone without plasticity is fixed. The systematic study on the possible effects of different mutations will be the object of future work—in particular, the effect of mutant clones on fluctuations, using SSA and within the linear noise approximation [22].

Recently, there has been experimental evidence that shows the existence of heterogeneity in the SC population [41], and a compartmental model [42] which includes this heterogeneity has been developed. The dynamics proposed in this model is similar to a Moran process, and does not allow consideration of fluctuations in cell population. Our intention in future work is to include heterogeneity in the population of SCs within the assumptions of the present work.

## Acknowledgments

This work was partially supported by PIO 144-2014-0100016-CO (CONICET—Argentina).

## Appendix A. Gillespie algorithm (SSA)

In order to make this article self-contained, and to save the reader from referring directly to [38], we present here a brief summary of the algorithm, as well as some details for this specific case.

Let us consider that the evolution of populations $S$ and $T_1$ are the result of a stochastic process consisting of the occurrence of six independent events with a given probability. The events, the probabilities of occurrence and the changes that occur in the populations involved are detailed below, when all SCs and $TAC_1$s are equally adapted.

(i) SC–SC Symmetric division of a SC:

$$\begin{aligned} P_{S,S} &\propto M_{S,S} S = a(1)\,, \\ S &\to S + 1\,, \\ T_1 &\to T_1\,. \end{aligned} \tag{A.1}$$

(ii) $TAC_1$–$TAC_1$ symmetric division of a SC:

$$\begin{aligned} P_{S,S} &\propto M_{T_1,T_1} S = a(2)\,, \\ S &\to S - 1\,, \\ T_1 &\to T_1 + 2\,. \end{aligned} \tag{A.2}$$

(iii) SC apoptosis:

$$\begin{aligned} P_{A_S} &\propto A_S S = a(3)\,, \\ S &\to S - 1\,, \\ T_1 &\to T_1\,. \end{aligned} \tag{A.3}$$

(iv) Plasticity:

$$\begin{aligned} P_P &\propto P T_1 = a(4)\,, \\ S &\to S + 1,\,, \\ T_1 &\to T_1\,. \end{aligned} \tag{A.4}$$

(v) $TAC_2$–$TAC_2$ symmetric division of a $TAC_1$:

$$\begin{aligned} P_{\mathrm{TAC}_2,\mathrm{TAC}_2} &\propto L_{T_1} T_1 = a(5)\,, \\ S &\to S\,, \\ T_1 &\to T_1 - 1\,. \end{aligned} \tag{A.5}$$

(vi) $TAC_1$ apoptosis:

$$\begin{aligned} P_{A_{T_1}} &\propto A_{T_1} T_1 = a(6)\,, \\ S &\to S\,, \\ T_1 &\to T_1 - 1\,. \end{aligned} \tag{A.6}$$

Once the event in the step is defined, the clone participating in it is determined by another stochastic

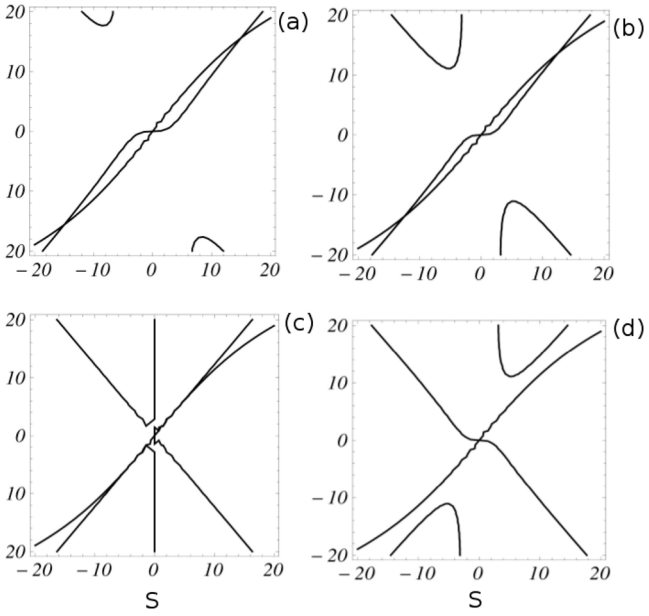


**Figure B1.** (a) Nullclines for normal crypt. (b) Nullclines for fixed mutant clone with $0 < m_1' < 1$. (c) Nullclines for $m_1' = 0$. (d) Nullclines for $m_1' < 0$.

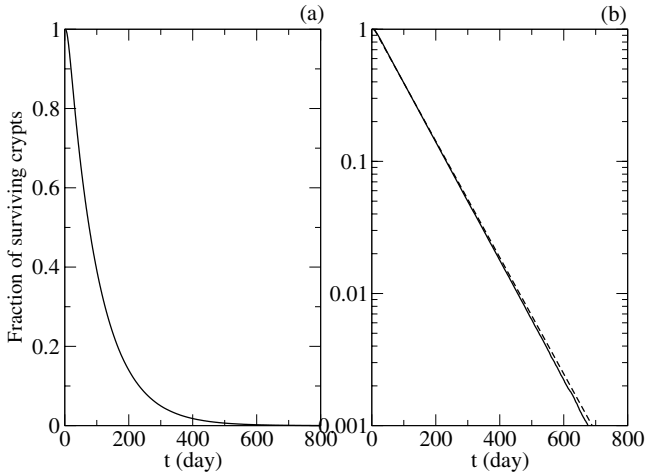


**Figure B2.** (a) Fraction of surviving crypts versus time. (b) The same as in (a) but in log–lin scale. The dashed line corresponds to the best exponential fit.

process. The probability that a cell of clone $j$ is involved is proportional to $s_j$ for SCs and to $t_j$ for $TAC_1$s. We discard the probability of simultaneous events, and the time between steps $\Delta t$ is calculated from the probability density $P(\Delta t) = \exp(-\Delta t \sum_i a(i))$.

For possible mutations of clone 15, it is assumed that the probability of participation in each event of that clone is proportional to $m_i s_{15}$, $(i = 1, 2, 3)$ for SCs and $m_i' t_{15}$, $(i = 1, 2, 3)$, while if $j \neq 15$ it remains proportional to $s_j$ or $t_j$.

If we suppose that the regulatory factors of each event (equations (9)–(15)) do not vary (this depends on the total number of SCs or $TAC_1$s); this implies that to include the mutations, we must only replace $S$ and $T_1$ by $\sum_j^{14} s_j + m_i s_{15}$ in $a(i)$, $(i = 1, 2, 3)$ in equations (A.1)–(A.3) and $\sum_j^{14} t_j + m_i' t_{15}$ in $a(i)$, $(i = 4, 5, 6)$ in equations (A.4)–(A.6) respectively.

## Appendix B. Nullclines

### B.1. Normal crypts

Here, we show the nullclines corresponding to the equations describing the evolution of SCs and $TAC_1$; equations (1) and (2) for the case when all cells are identical with the parameters shown in table 1. The nullcline corresponding to $dT_1/dt = 0$ is a simple curve, whereas that corresponding to $dS/dt = 0$ is multivalued. One of the solutions is a curve that passes through the origin, while the other one similar

to a hyperbola, with two branches. The region of biological interest is reduced to the first quadrant ($S \geqslant 0, T_1 \geqslant 0$). There are two possible points of equilibrium. One of these, ($S_s = 15, T_{s1} = 15.62$), is stable, while the other, ($S_s = 0, T_{s1} = 0$), is unstable (see figure B1(a)).

### B.2. Crypts with a fixed mutant clone

As we have seen in section 4, to study the evolution towards monoclonality it is necessary to abandon the continuous description of the differential equations. However, once a clone is fixed (whether mutant or not), the differential equations acquire some meaning, since they describe the average behavior of the populations. If the prevailing clone is normal, the differential equations have the same parameters given by table 1. If, instead, the mutant clone is fixed, the parameters change according to the effect of the mutation. In particular, if the mutation is such that plasticity changes, $P \to m_1' P$.

Changes in the parameters modify the nullclines and thus the possible equilibrium points for the populations. The figure B1(b) shows the nullclines corresponding to a mutation with decreasing plasticity. For this mutation, the nullcline corresponding to $\mathrm{d}T_1/\mathrm{d}t = 0$ does not change, but that to $\mathrm{d}S/\mathrm{d}t = 0$ does. So the values for the equilibrium of populations ($S_s$ and $T_{s1}$) decrease. We can also see how the two branches of the hyperbolic nullcline approach the origin. In figure B1(c), we show the limiting case, in which the fixed clone has no plasticity. In this case, we see how the stable equilibrium point disappears and the hyperbolic solution degenerates in its asymptotes. This means if the mutant clone is set, the crypt is extinguished. Mathematically, this case ($P = 0$) corresponds to a bifurcation. For completeness, we show in figure B1(d) the nullclines for $P < 0$ (which have no biological sense).

## Appendix C. Extinction by fluctuations

To describe the evolution of populations by means of differential equations, it is important to verify the stability of the solutions not only under parameter fluctuations, but also against the fluctuations coming from a stochastic problem of losses and profits. If steady-state solutions involve large populations, this may be irrelevant but when considering small colonies (as in the case of crypts), it is mandatory. As an example, we compare the solution of the differential equation for the evolution for the SCs population ($N_0$) proposed for a compartment model of crypts [39] with the solution of the same through the algorithm shown in the previous appendix:

$$\frac{\mathrm{d}N_0}{\mathrm{d}t} = (\alpha_3 - \alpha_1 - \alpha_2)N_0 - \frac{k_0 N_0^2}{1 + m_0 N_0}. \qquad \text{(C.1)}$$

For normal crypts, the authors set $\alpha_1 = 0.1$, $\alpha_2 = 0.3, \alpha_3 = 0.686, k_0 = 0.1, m_0 = 0.1$. With these parameters, the equation has a fixed point at $N_{s0} = 4$. However, when solving the equation with the stochastic algorithm it is clear that the crypts extinguish exponentially with a half life of 98.63 d, as can be seen in figure B2. Let us remark that the extinction of crypts is an event that normally occurs rarely [40]: the extinction rate is much less than $10^{-3}\,\mathrm{d}^{-1}$

## ORCID iDs

A J Fendrik https://orcid.org/0000-0001-8934-8668

## References


[1] Itzkovitz S, Blat I C, Jacks T, Clevers H and van Oudenaarden A S 2012 Optimality in the development of intestinal crypts *Cell.* **148** 608–19

[2] Takahashi T, Nowakowski R S and Caviness V S Jr 1996 The leaving or Q fraction of the murine cerebral proliferative epithelium: a general model of neocortical neurogenesis *J. Neurosci.* **16** 6183–96

[3] Barton A, Fendrik A J and Rotondo E 2014 A stochastic model of neurogenesis controlled by a single factor *J. Theor. Biol.* **355** 77–82

[4] Klein A M and Simons B D 2011 Universal patterns of stem cell fate in cycling adult tissues *Development* **138** 3103–11

[5] Potten C S and Loeffler M 1990 Stem cells: attributes, cycles, spirals, pitfalls and uncertainties. Lessons for and from the crypt *Development* **110** 1001–20

[6] Paulus U, Potten C S and Loeffler M 1992 A model of the control of cellular regeneration in the intestinal crypt after perturbation based solely on local stem cell regulation *Cell Proliferation* **25** 559–78

[7] Marshman E, Booth C and Potten C S 2002 The intestinal epithelial stem cell *BioEssay* **24** 91–6

[8] Ouellette A J 2015 Defensins in enteric mucosal immunity *Mucosal Immunology* vol 1, ed J Mestecky *et al* 4th edn (New York: Academic) pp 271–86

[9] Carrol T D, Langlands A J, Osborne J M, Newton P, Appleton P L and Nathke I S 2017 Interkinetic nuclear migration and basal tethering facilitates post-mitotic daughter separation in intestinal organoids *J. Cell Sci.* **130** 3862–77

[10] Alberts B, Johnson A, Lewis J, Raff M, Roberts K and Walter P 2008 *Molecular Biology of the Cell* 5th edn (New York: Garland Science) ch 23

[11] van der Fliers L G and Clevers H 2009 Stem cells, self-renewal and differentiation in the intestinal epithelium *Annu. Rev. Physiol.* **71** 241–60

[12] Paulus U, Loeffler M, Zeidler J, Owen G and Potten C S 1993 The differentiation and lineage development of globet cells in the murine small intestinal crypt: experimental and modelling studies *J. Cell Sci.* **106** 473–83

[13] Li Y Q, Roberts S A, Paulus U, Loeffler M and Potten C S 1994 The crypt cycle in mouse small intestinal epithelium *J. Cell Sci.* **107** 3271–9

[14] Yatabe Y, Tavar S and Shibata D 2001 Investigating stem cells in human colon by using methylation patterns *PNAS* **98** 10830–44

[15] Potten C S, Booth C, Tudor G L, Booth D, Brady G, Hurley P, Ashton G, Clarke R, Shin-Ichi S and Hideyuki O 2003 Identification of a putative intestinal stem cell and early linage marker musashi-1 *Differentiation* **71** 28–41

[16] Barker N *et al* 2007 Identification of stem cells in small intestine and colon by marker gene Lgr5 *Nature* **449** 1005–7

[17] Drasdo D and Loeffler M 2001 Individual-based models to growth and folding in one-layered tissues: intestinal crypts and early development *Nonlinear Anal.* **47** 245–56

[18] Levin B, Rozen P and Young G P 2002 How should we follow up colorectal premalignant conditions? *Colorectal Cancer in Clinical Practice: Prevention, Early Detection and Management* ed P Rozen *et al* (London: Martin Dunitz Ltd) pp 67–76
[19] Ro S and Rannala B 2001 Methylation patterns and mathematical models reveal dynamics of stem cell turnover in the human colon *Proc. Natl Acad. Sci.* **98** 10519–21
[20] Katz J P, Perreault N, Goldstein B G, Lee C S, Labosky P A, Yang V W and Kaestner K H 2002 The zinc-finger transcription factor Klf4 is required for terminal differentiation of globet cells in the colon *Development* **129** 2619–28
[21] Tsimring L S 2014 Noise in biology *Rep. Prog. Phys.* **77** 1–62
[22] Schnoerr D, Sanguinetti G and Grima R 2017 Approximation and inference methods for stochastic biochemical kinetics-a tutorial review *J. Phys. A: Math Theor.* **50** 093001–80
[23] Baker A-M *et al* 2014 Quantification of crypt and stem cell evolution in the normal and neoplatic human colon *Cell Rep.* **8** 940–7
[24] Snippert H J *et al* 2010 Intestinal crypt homeostasis results from neutral competition between symmetrically dividing Lgr5 stem cells *Cell* **143** 134–44
[25] Lopez-Garcia C, Klein A M, Simons B D and Winton D J 2010 Intestinal stem cell replacement follows a pattern of neutral drift *Science* **330** 822–5
[26] Simons B D and Clevers H 2011 Stem cell self-renewal in intestinal crypt *Exp. Cell. Res.* **317** 2719–24
[27] van Leeuwen I, Byrne H, Jensen O and King J 2007 Elucidating the interactions between the adhesive and transcriptional functions of ß-catenin in normal and cancerous cells *J. Theor. Biol.* **247** 77–102
[28] Pitt-Francis J *et al* 2009 Chaste: a test-driven approach to software development for biological modelling *Comput. Phys. Commun.* **180** 2452–71
[29] Mirams G R, Fletcher A G, Maini P K and Byrnea H M 2012 A theoretical investigation of the effect of proliferation and adhesion on monoclonal conversion in the colonic crypt *J. Theor. Biol.* **312** 143–56
[30] Fletcher A G, Breward C J W and Chapman S J 2012 Mathematical modeling of monoclonal conversion in the colonic crypt *J. Theor. Biol.* **300** 118–33
[31] Kang H and Shibata D 2013 Direct measurement of human colon crypt stem cell niche genetic fidelity: the role of chance in non-darwinian mutation selection *Front. Oncol.* **3** 264–10
[32] van Leeuwen I I M, Byrne H M, Jensen O E and King J R 2006 Crypt dynamics and colorectal cancer: advances in mathematical modelling *Cell Proliferation* **39** 157–81
[33] De Matteis G, Graudenzi A and Antoniotti M 2013 A review of spatial computational models for multi-cellular systems, with regard to intestinal crypts and colorectal cancer development *J. Math. Biol.* **66** 1409–62
[34] Carulli A J, Samuelson L C and Schnell S 2014 Unraveling intestinal stem cell behavior with models of crypt dynamics *Integr. Biol.* **6** 243–57
[35] Fletcher A G, Murray P J and Maini P K 2015 Multiscale modelling of intestinal crypt organization and carcinogenesis *Math. Models Methods Appl. Sci.* **3** 2563–8
[36] Parker A, Mclaren O J, Fletcher A G, Murano D, Kreuzaler P A, Byme H M, Maini P K, Watson A J M and Pin C 2017 Cell proliferation within small intestinal crypts is the principal driving force for cell migration on villi *FASEB J.* **31** 636–49
[37] Maclaren O J, Carding S R, Fletcher A G and Maini P A hierarchical Bayesian model for understanding the spatiotemporal dynamics of the intestinal epithelium 2017 *PLoS Comput. Biol.* **13** 1005688
[38] Gillespie D T 1977 Exact stochastic simulation of coupled chemical reactions *J. Phys. Chem.* **81** 2340–61
[39] Johnston M D, Edwards C M, Bodmer W F, Maini P K and Chapman S J 2007 Mathematical modeling of cell population dynamics in the colonic crypt and in colorectal cancer *Proc. Natl Acad. Sci.* **104** 4008–13
[40] Loeffler M and Grossmann B 1991 A stochastic branching model with formation of subunits applied to the growth of intestinal crypts *J. Thoer. Biol.* **150** 175–91
[41] Ritsma L, Ellenbroek S I J, Zomer A, Snippert H J, de Sauvage F J, Simons B D, Clevers H and van Rheenen J 2014 Intestinal crypt homeostasis revealed atsingle-stem-cell level by in vivo live imaging *Nature* **507** 362–5
[42] Shahriyari I and Mahdipour-Shirayeh A 2017 Modeling dynamics of mutants in heterogeneous stem cell niche *Phys. Biol.* **14** 016004